Received 10 March 2025; accepted 10 April 2025. Date of publication 15 April 2025;
date of current version 28 April 2025.

Digital Object Identifier 10.1109/OJUFFC.2025.3560938

Evaluation of a Dual Linear Flexible Ultrasound Array for Surgical Interventional Guidance

HASTI ROSTAMIKHANGHAHI[1], MARCUS INGRAM[1], BRIAN G. BOOTH[2], AND JAN D'HOOGE[1]

[1]Department of Cardiovascular Imaging and Dynamics, KU Leuven, 3000 Leuven, Belgium
[2]imec TELIN–IPI, Ghent University, 9000 Ghent, Belgium

CORRESPONDING AUTHOR: H. ROSTAMIKHANGHAHI (hasti.rostamikhanghahi@kuleuven.be)

This work was supported by the Fonds Wetenschappelijk Onderzoek (FWO) under the "HoloWrist" Project under Grant G0A8721N.

ABSTRACT Scaphoid fractures, the most common of wrist bone fractures, are typically treated using Percutaneous Scaphoid Fixation (PSF). Incorporating ultrasound guidance into this technique could reduce reliance on fluoroscopy, thereby avoiding ionizing radiation and improving procedural accuracy. However, the scaphoid's position can shift as a result of hand movement during PSF, adding complexity to the procedure. Real-time ultrasound motion tracking of the scaphoid during PSF could simplify the intervention, which would necessitate a flexible transducer array to maintain contact during wrist motion. Our previous research proposed a transducer design with two parallel flexible 1D arrays, enabling simultaneous acquisition of two parallel images. This study focuses on transitioning from theoretical design to practical application by evaluating the performance of the custom array in terms of image quality using phantoms. We assessed image quality using the generalized contrast-to-noise ratio (gCNR) on a cyst phantom and the full width at half maximum (FWHM) on a wire phantom. Results demonstrated gCNR values above 0.67 and FWHM values below 0.70 mm across all sequences. These measurements fall within the acceptable range for the phantoms. Since the primary goal of the array is to track the scaphoid bone during surgery, requiring relatively high image quality, the values observed in this study are suitable for this application.

INDEX TERMS Flexible ultrasound array, percutaneous scaphoid fixation, ultrasound tracking of the scaphoid.

I. INTRODUCTION

ULTRASOUND (US) imaging is a diagnostic technique that offers several key advantages, such as being cost-effective and non-invasive. Unlike X-ray (XR) imaging, US does not involve ionizing radiation, making it a safer option for patients. For example, in pediatric cases, US enables the study of the cartilaginous components of immature bones, which are difficult to evaluate with XR and remain a significant diagnostic challenge [1], [2]. Additionally, in cases of non-displaced torus forearm fractures (Buckle fractures) and ''greenstick'' fractures, US has proven to be as effective as XR for both diagnosis and management [3].

Flexible US transducer arrays have been developed in medical applications and have greatly improved wearable ultrasound devices. Wang et al. developed a wearable ultrasound transducer array that can be applied directly to the skin, allowing for continuous monitoring of central blood pressure [4]. This wearable array offers several key benefits over current methods, such as fitting to the skin, having a compact design, and delivering high accuracy. Pashaei et al. developed flexible, linear transducer arrays by integrating matrices of PZT elements onto a flexible printed circuit board (PCB) for use in image-guided neural modulation [5]. These arrays were designed to be bendable and were worn directly on a volunteer's neck. Du et al. developed a conformable ultrasound breast patch for imaging and scanning breast tissue, addressing limitations of traditional ultrasound systems, such as operator dependence and challenges with curved surfaces [6]. By integrating a honeycomb-inspired patch with a phased-array transducer, the device enables large-area, deep-tissue imaging. This noninvasive solution offers a practical approach to early breast cancer detection. Hu et al. presented

a novel wearable cardiac ultrasound device designed for continuous, real-time monitoring of cardiac function, overcoming the limitations of traditional echocardiography [7]. The device incorporates advanced material fabrication to maintain close skin contact and deliver high-quality imaging during motion.

While flexible array technologies have been explored in various medical applications [4], [5], [6], [7], there have been no studies specifically focused on wearable devices for the wrist and, in particular, Percutaneous Scaphoid Fixation (PSF) surgery. To address this gap, we previously designed and simulated a dual linear flexible ultrasound array for real-time tracking of the scaphoid during PSF [8]. The 'dual array' configuration, featuring two parallel 1D arrays in a single housing, was selected as an optimal balance between array control complexity and its capability to provide elevational information. The designed array was then manufactured by Olympus (MA, USA).

The aim of this study is to evaluate the performance of this dual linear flexible ultrasound array specifically designed for real-time scaphoid tracking during PSF. The objective is to transition the design from a theoretical concept to practical application by assessing the bespoke array performance through experimental analysis. In this study, we evaluated different imaging sequences using phantoms, including linear-stepped scan modes (both flat and curved configurations) and plane wave imaging, to assess image quality. The novelty of this work lies in the flexibility of our array, introducing a novel approach to imaging, particularly for wrist applications and this specific surgical procedure.

This paper is organized as follows: Section II outlines the transducer and experimental setups used to assess imaging performance. In Section III, we present the results of the array evaluation, focusing on image quality. Finally, our conclusions are drawn in Section IV.

II. MATERIALS AND METHODS

A. TRANSDUCER SETUP

The probe utilizes a dual linear flexible configuration, featuring two parallel 1D arrays within a single housing (Fig. 1a). Each array consists of 64 elements with a center frequency of 7.5 MHz and an element pitch of 1.5λ (0.30 mm). This configuration allows for the simultaneous acquisition of two parallel images, facilitating precise scaphoid tracking during PSF.

B. EXPERIMENTAL SETUP

A wire phantom (Model 055, CIRS, VA, USA) [9] and a cyst phantom (Model 040GSE, CIRS, VA, USA) [10] were used for the experiments. The arrays were controlled by our Ultrasound Advanced Open Platform (ULA-OP 256) [11]. The transducer was tested with two different sequences to evaluate image quality:

1. The two arrays were used sequentially in linear scan mode, each with a sub-aperture size of 16 elements,

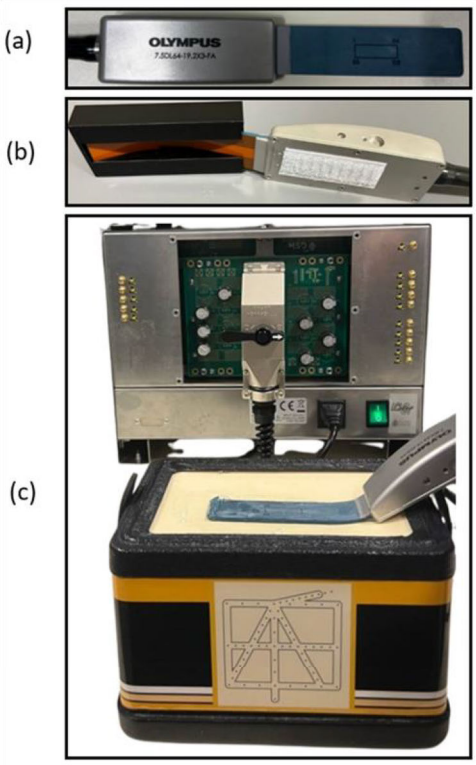

FIGURE 1. Setup for the experiment a) array b) array curved with 3D holder c) array flat on the wire phantom controlled by ultrasound scanner.

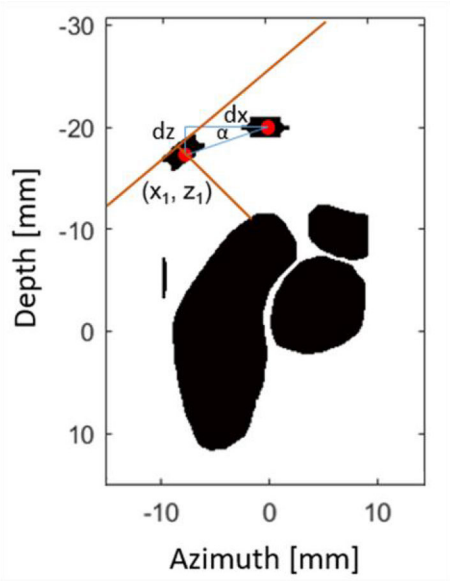

FIGURE 2. Schematic illustrating the process of calculating focal points.

generating two parallel images. The first sub-aperture started from the first element, advancing in steps of one element, resulting in a 15-element overlap between consecutive sub-apertures. Consequently, each array had 49 sub-apertures, resulting in 49 transmits per array, totaling 98 transmits overall. For this sequence,

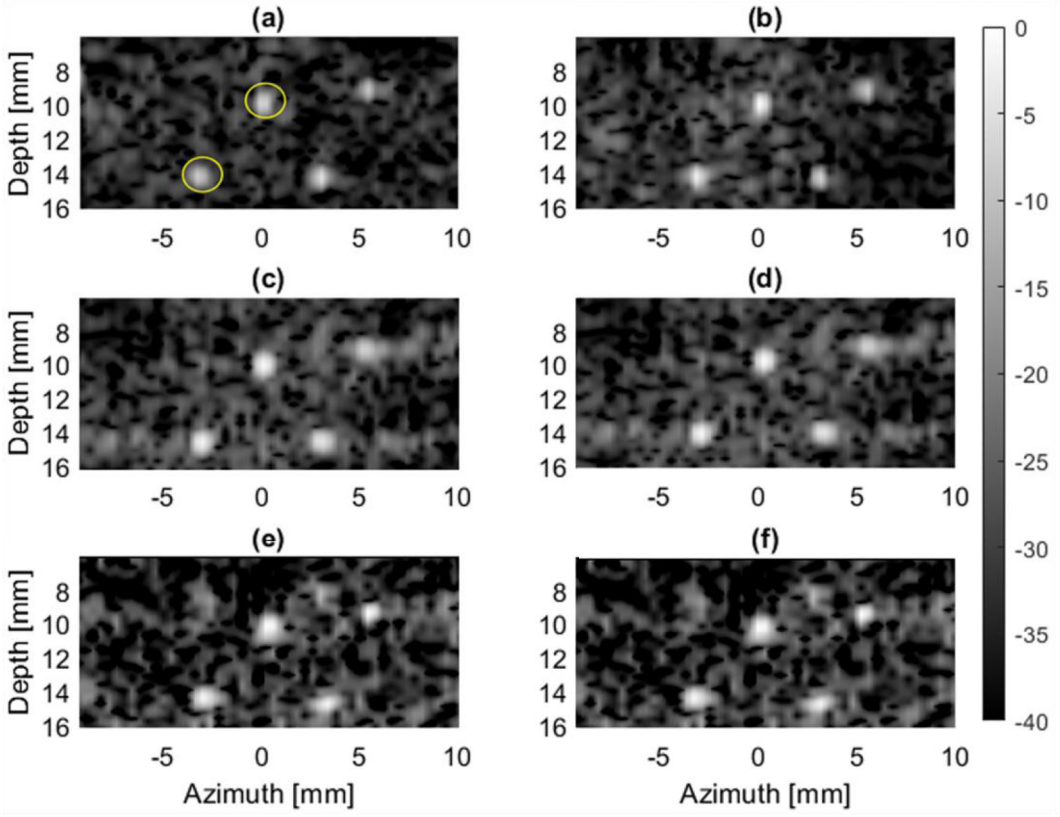

FIGURE 3. **B-mode images of the wire phantom by: first array a) flat on the phantom using linear-stepped scan c) curved using a 3D holder using linearsteppedscan e) reconstructed by all elements transmitting 5 plane waves at the same time; and second array b) flat on the phantom using a linearsteppedscan d) curved using a 3D holder with a linear-stepped scan f) reconstructed by all elements transmitting 5 plane waves at the same time.**

the array was used in two configurations: initially, it was placed flat on the phantom, and subsequently, it was flexed using a 3D-printed holder corresponding to the curvature of an average human wrist (Fig. 1b). The known shape of the array was used to calculate both the transmit and receive delays.

2. All elements of the transducer simultaneously transmitted plane waves. We used five plane waves with different transmit angles ($-5.2°, -2.6°, 0°, 2.6°, 5.2°$), which were incorporated during the compounding process. Each angled wave insonified the phantom, and the resulting echoes were collected and stored separately. This produced a set of individual images, each representing the scene from a slightly different perspective. These images were then compounded, resulting in two final images—one from each aperture.

In this experiment, we did not use steering in our linear-stepped sequence and employed small transmit angles in our plane wave sequence primarily to mitigate the effects of grating lobes. Fig. 1c shows the setup used in the experiments.

C. CALCULATION OF FOCAL POINTS IN A CURVED ARRAY

When using a flat array, the focal points are directly below the aperture at the focal distance. However, for a curved array, the focal point of each sub-aperture lies along a line perpendicular to the apex of that sub-aperture. Therefore, we need to calculate the focal points accordingly. Fig. 2 shows the scaphoid and a few of other carpal bones in the imaging scene. Consider the calculation of the focus point for the first sub-aperture: The red dot on the left is the apex for first sub-aperture (x_1,z_1) and the red dot on the right is the apex for middle sub-aperture. The parameters dx and dz represent the differences in the coordinates between the apices of the sub-apertures along the x and z axes, respectively. As shown in Fig. 2, the angle (α) between the sub-apertures can be determined using dx and dz. Given this angle and the length of the array, the radius of curvature (R) can be known. Using the radius of curvature and the coordinates of the apex of the first sub-aperture, the normal vector components for the current sub-aperture are computed as follows:

$$n_x = cos\,(arctan\,(normal\ slope)) = \frac{1}{\sqrt{1+\left(\frac{R^2-x_1^2}{x_1^2}\right)}} \quad (1)$$

$$n_z = \sin(arctan(normal\ slope)) = \frac{\sqrt{R^2-x_1^2}}{x_1.\sqrt{1+\left(\frac{R^2-x_1^2}{x_1^2}\right)}} \quad (2)$$

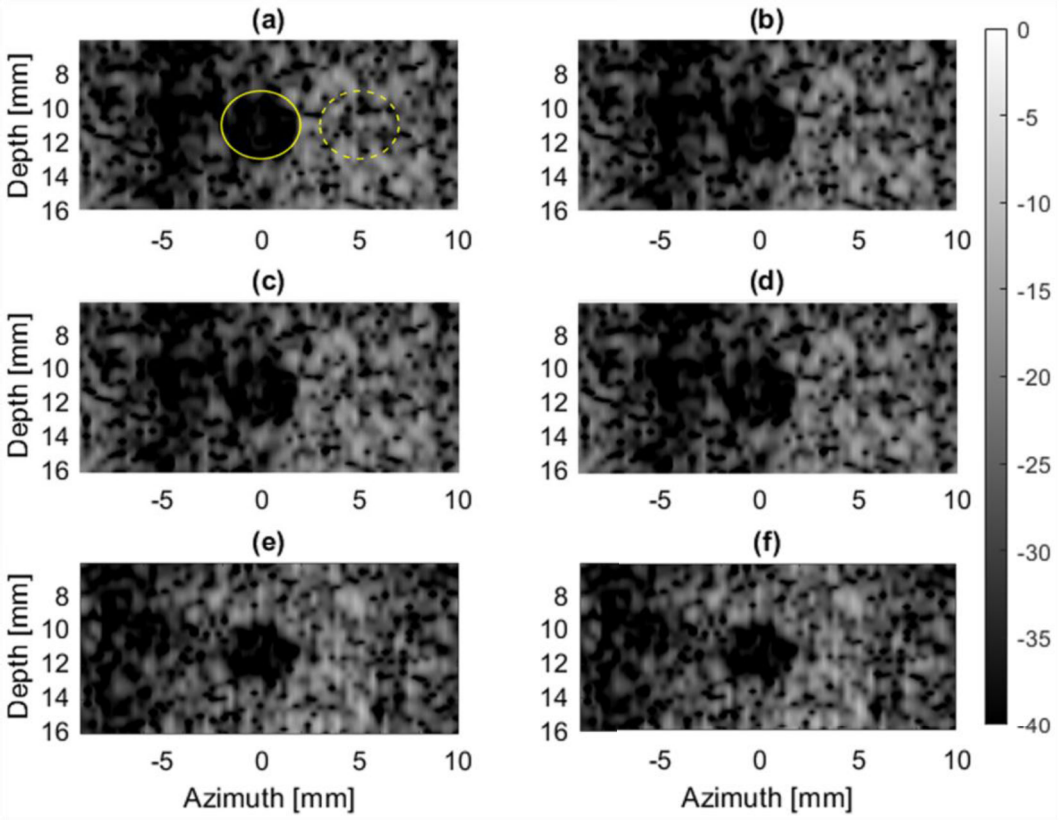

FIGURE 4. **B-mode images of the anechoic cyst by: first array a) flat on the phantom using linear-stepped scan c) curved using a 3D holder using linearsteppedscan e) reconstructed by all elements transmitting 5 plane waves at the same time; and second array b) flat on the phantom using a linearsteppedscan d) curved using a 3D holder with a linear-stepped scan f) reconstructed by all elements transmitting 5 plane waves at the same time.**

which we can then use to calculate the focus point using the normal vector and focal depth

$$x = focal\ depth.n_x = \frac{focal\ depth}{\sqrt{1+\left(\frac{R^2-x_1^2}{x_1^2}\right)}} \tag{3}$$

$$z = focal\ depth.n_z = \frac{focal\ depth.\sqrt{R^2-x_1^2}}{x_1.\sqrt{1+\left(\frac{R^2-x_1^2}{x_1^2}\right)}} \tag{4}$$

$$focus\ point = (x_1 - x, 0, z_1 - z) \tag{5}$$

D. METRICS

To quantitatively assess the performance of the arrays, we measured the generalized contrast-to-noise ratio (gCNR) [12] and the full width at half maximum (FWHM).

1. **Generalized Contrast-to-Noise Ratio (gCNR)**
   Essentially, gCNR quantifies image contrast and can be interpreted as the probability of an ideal viewer successfully distinguishing between pixels. The gCNR improves upon the traditional CNR by considering the intersecting region of two probability density functions. This advanced measure of contrast-to-noise ratio remains stable despite changes in dynamic range and can be applied to images of any type, scale, or unit. The gCNR is measured using the following formula:

$$gCNR = 1 - \int min\left(p_{bkg(x)}, p_{trgt(x)}\right) dx \tag{6}$$

   $p_{bkg(x)}$ and $p_{trgt(x)}$ represent the probability density functions of the intensity in the background and target regions, respectively. We evaluated the gCNR on an anechoic cyst positioned at the center of the active aperture and located at the typical focal position for the scaphoid.
2. **Full Width at Half Maximum (FWHM)**
   FWHM is a key metric for assessing lateral resolution in ultrasound imaging. It measures the width of the ultrasound beam at half of its maximum amplitude, directly indicating the system's ability to distinguish between side-by-side objects. Lateral resolution, which is measured perpendicular to the beam direction, is derived from the beam profile by calculating the FWHM. A smaller FWHM value implies better lateral resolution, thereby enhancing the clarity and detail of the ultrasound image. We assessed the FWHM on two wires, one of

TABLE 1. Table of results.

	1st array	2nd array	1st array	2nd array	1st array	2nd array
Sequence / Metrics	Linear stepped-flat array		Linear stepped-curved array		Plane wave	
gCNR	0.87	0.87	0.79	0.79	0.67	0.67
FWHM (mm) @10 mm	0.50	0.47	0.55	0.50	0.55	0.55
FWHM (mm) @14 mm	0.60	0.50	0.68	0.65	0.70	0.70

them positioned at the center of the active aperture, another one 3 mm off the center, both located around the typical focal position for the scaphoid.

III. RESULTS

Fig. 3 and Fig. 4 show B-mode images of both arrays for the different sequences described earlier for wires and an anechoic cyst. Fig. 3a shows the regions of interest used for measuring the FWHM, marked by two 1 mm radius circles: one centered at (0,10) and the other at (−3,14). Similarly, Fig. 4a highlights the regions of interest used to define the gCNR, with the solid circle centered at (0,11) representing the target region and the dashed circle centered at (5,11) representing the background region. Table 1 presents the gCNR and FWHM values for both arrays across different sequences.

IV. CONCLUSION

Flexible arrays have recently been developed for medical applications, advancing wearable ultrasound devices. However, there have been no studies specifically focused on wearable devices for the wrist, particularly in the context of Percutaneous Scaphoid Fixation (PSF) surgery. In this study, we evaluated the image quality of a flexible ultrasound array, previously designed in our earlier research, for tracking the scaphoid during PSF. We demonstrated the overall image quality of the array and evaluated its performance by curving it with a 3D holder. The resulting images were compared in terms of quality to those obtained from the flat configuration of the same array, as well as to images acquired using a plane wave imaging sequence. Our results demonstrate gCNR values consistently above 0.67, reaching a maximum of 0.87, and FWHM values below 0.70 mm, with a minimum of 0.47 mm. Additionally, when comparing the image quality of the array in its curved configuration to that of the flat array and the plane wave sequence, the curved images appear promising. These measurements fall within the acceptable range for our phantoms. As previously mentioned, the primary goal of this array is to track the scaphoid bone during surgery, requiring relatively good image quality. The values observed in this study are suitable for this application.

REFERENCES

[1] J. A. Nicholson, S. T. J. Tsang, T. J. MacGillivray, F. Perks, and A. H. R. W. Simpson, "What is the role of ultrasound in fracture management?" *Bone Joint Res.*, vol. 8, no. 7, pp. 304–312, Jul. 2019.

[2] B. K. Weeks, R. Hirsch, R. C. Nogueira, and B. R. Beck, "Is calcaneal broadband ultrasound attenuation a valid index of dual-energy X-ray absorptiometry-derived bone mass in children?" *Bone Joint Res.*, vol. 5, no. 11, pp. 538–543, Nov. 2016.

[3] D. Williamson, "Ultrasound imaging of forearm fractures in children: A viable alternative?" *Emergency Med. J.*, vol. 17, no. 1, pp. 22–24, Jan. 2000.

[4] C. Wang et al., "Monitoring of the central blood pressure waveform via a conformal ultrasonic device," *Nature Biomed. Eng.*, vol. 2, no. 9, pp. 687–695, Sep. 2018.

[5] V. Pashaei, P. Dehghanzadeh, G. Enwia, M. Bayat, S. J. A. Majerus, and S. Mandal, "Flexible body-conformal ultrasound patches for image-guided neuromodulation," *IEEE Trans. Biomed. Circuits Syst.*, vol. 14, no. 2, pp. 305–318, Apr. 2020.

[6] W. Du et al., "Conformable ultrasound breast patch for deep tissue scanning and imaging," *Sci. Adv.*, vol. 9, no. 30, Jul. 2023, Art. no. eadh5325.

[7] H. Hu et al., "A wearable cardiac ultrasound imager," *Nature*, vol. 613, no. 7945, pp. 667–675, Jan. 2023.

[8] H. Rostamikhanghahi, M. Ingram, B. G. Booth, and J. D'hooge, "Design of a linear flexible ultrasound array transducer for real-time tracking of the scaphoid during percutaneous scaphoid fixation," in *Proc. IEEE Int. Ultrason. Symp. (IUS)*, Sep. 2023, pp. 1–3.

[9] CIRS. *Wire Phantom Model 055*. Computerized Imaging Reference Systems, Norfolk, VA, USA. Accessed: Jan. 10, 2025. [Online]. Available: https://www.cirsinc.com/products/ultrasound/ultrasound-phantoms-for-2d-3d-evaluation

[10] CIRS. *Multi-Purpose Multi-Tissue Ultrasound Phantom Model 040GSE*. Computerized Imaging Reference Systems, Norfolk, VA, USA. Accessed: Jan. 10, 2025. [Online]. Available: https://www.cirsinc.com/products/ultrasound/multi-purpose-multi-tisse-ultrasound-phantom/

[11] D. Mazierli, A. Ramalli, E. Boni, F. Guidi, and P. Tortoli, "Architecture for an ultrasound advanced open platform with an arbitrary number of independent channels," *IEEE Trans. Biomed. Circuits Syst.*, vol. 15, no. 3, pp. 486–496, Jun. 2021.

[12] A. Rodriguez-Molares et al., "The generalized contrast-to-noise ratio: A formal definition for lesion detectability," *IEEE Trans. Ultrason., Ferroelectr., Freq. Control*, vol. 67, no. 4, pp. 745–759, Apr. 2020.